The Predictability from Skull Morphology of Temporalis and Masseter Muscle Cross-Sectional Areas in Humans

VIVIANA TORO-IBACACHE,[1,2]* VICTOR ZAPATA MUÑOZ,[3] AND PAUL O'HIGGINS[1]

[1]Department of Archaeology and Hull York Medical School, Centre for Anatomical and Human Sciences, University of York, Heslington, York, United Kingdom
[2]Facultad de Odontología Universidad de Chile, Independencia, Región Metropolitana, Chile
[3]Centro de Imagenología, Hospital Clínico Universidad de Chile, Independencia, Región Metropolitana, Chile

ABSTRACT

To carry out functional simulations of the masticatory system that aim to predict strain magnitudes it is important to apply appropriate jaw-elevator muscle forces. Force magnitude estimation from directly measured muscle physiological cross-sectional area or anatomical cross-sectional area (CSA) is not possible for fossils and skeletal material from museum collections. In these cases, muscle CSAs are often estimated from bony features. This approach has been shown to be inaccurate in a prior study based on direct measurements from cadavers. Postmortem alterations as well as age changes in muscle form might explain this discrepancy. As such, the present study uses CT images from 20 living individuals to directly measure temporalis and masseter muscle CSAs and estimated cross-sectional areas (ECSAs) from bony features. The relationships between CSAs and ECSAs were assessed by comparing mean values and by examining correlations. ECSAs are up to 100% greater than CSA and the means of these variables for each muscle differ significantly. Further, ECSA is significantly correlated with CSA for temporalis but not masseter. Cranial centroid size is only significantly associated with CSA for temporalis. These findings indicate that ECSAs should be employed with caution in simulations of human masticatory system functioning; they do not reflect CSAs and it is plausible that this also applies to studies of closely related living and fossil taxa. When ECSAs are used, sensitivity analyses are required to determine the impact of potential errors. Anat Rec, 298:1261–1270, 2015. © 2015 Wiley Periodicals, Inc.

Key words: muscle cross-sectional area; dry skull method of muscle area estimation; skull size; computed tomography

Grant sponsor: Comisión Nacional de Investigación Científica y Tecnológica (Chile) (Becas Chile) (to V.T.-I.).

*Correspondence to: Viviana Toro-Ibacache, Facultad de Odontología, Universidad de Chile, Sergio Livingstone Pohlhammer 943, Independencia, Región Metropolitana, Chile. E-mail: mtoroibacache@odontologia.uchile.cl

Received 11 September 2014; Revised 15 January 2015; Accepted 15 January 2015.

DOI 10.1002/ar.23156
Published online 23 April 2015 in Wiley Online Library (wileyonlinelibrary.com).

INTRODUCTION

During biting, the forces produced by the temporalis, masseter, and medial pterygoid muscles are key determinants of masticatory system performance. Additionally, these muscles apply forces to the masticatory system and the strains they generate in skeletal tissues are important in ensuring balanced growth (Scott, 1957; Moss, 1962; Yoshikawa et al., 1994; DiGirolamo et al., 2013). In simulating function, e.g. biting, using mechanical analysis such as finite element analysis, accurate muscle forces (Ross et al., 2005; Fitton et al., 2012; Gröning et al., 2012) are required to reliably predict performance parameters such as bite forces, skeletal stresses, and strains. In studies of dry skeletons or fossil material, muscle forces have to be estimated and this is frequently done using bony features (Demes and Creel, 1988; Antón, 1990; O'Connor et al., 2005; Wroe et al., 2010).

The maximum contractile force a muscle can generate can be estimated from its physiological cross-section area (PCSA). PCSA is defined as the total cross-sectional area of all muscle fibres at a specified muscle length, and muscle force is estimated as the product of PCSA and the intrinsic strength of the muscle (Weijs and Hillen, 1985a; Koolstra et al., 1988; O'Connor et al., 2005). PCSA measurement is based on anatomical dissection (Koolstra et al., 1988; van Eijden et al., 1997; Antón, 1999) or contrast-enhanced computed tomography (CT) (Cox and Jeffery, 2011). Both can be impractical, for instance in studies of material from skeletal collections. For humans, dissecting room specimens provide an opportunity to determine PCSA by dissection (Koolstra et al., 1988; Antón, 1994; van Eijden et al., 1997) but most commonly such material is from aged individuals who may have experienced masticatory muscle reduction due to either ageing, tooth loss, or both (Newton et al., 1993; Mioche et al., 2004). Further, the preservation process and/or postmortem changes may impact on muscle structure (see Martin et al., 2001 for postmortem changes in fiber length and pennation angle). In addition, cadaveric material is most commonly available only after it has been used for teaching, when it may be too damaged to perform direct muscle force estimation. However, computed tomography or magnetic resonance imaging (MRI) allows direct measurement in living subjects of muscle cross-sectional area (CSA; Weijs and Hillen, 1986; Hannam and Wood, 1989; van Spronsen et al., 1992). Although CSA does not take account of pennation it has been shown to correlate with PCSA in jaw-elevator muscles (Weijs and Hillen, 1984) and so, to offer a reasonable means of obtaining muscle force estimates. As noted earlier, when muscles are absent as is the case in studies based on skeletal specimens, bony proxies are commonly used to estimate CSA and muscle force, with the aim of inferring diet and ecology from masticatory mechanics (Demes and Creel, 1988; Antón, 1990; O'Connor et al., 2005; Wroe et al., 2010). Antón (1999) showed that PCSAs of jaw-elevator muscles have low predictability from bony proxies in macaques. The same author studied this relationship in 10 human cadavers, showing a lack of correlation between PCSAs and the sizes of masseter and medial pterygoid bone attachment areas. Further, she found a weak relationship between temporalis' PCSA and the anteroposterior length of the temporal fossa at the level of the zygomatic arch (Antón, 1994). To date, no studies have been performed in living humans comparing CSAs from CT scans with estimated CSAs from bony proxies.

The aim of this study is therefore to assess the relationship between muscle CSAs and muscle areas estimated from bony features visible in CT scans. Additionally, the relationship of both variables to skull centroid size is assessed in order to account for any general size effect (Weijs and Hillen, 1986; Seeman, 2001) and to assess predictability of muscle CSAs from this. Averages of measured CSAs are provided as reference data. Since our study is based on living individuals, direct measurement from bone was not possible, and we used virtual three-dimensional (3D) anatomical reconstruction techniques to estimate muscle cross-sectional areas (ECSAs). This approach is also appropriate for skeletal remains with adherent soft tissues and for virtually reconstructed fragmentary skulls such as fossils. Further, 3D reconstruction of crania for studies of masticatory system functioning is increasingly common, using methods such as finite element analysis (FEA) (Rayfield, 2007; Kupczik et al., 2009; Wroe et al., 2010) and multibody dynamic analysis (MDA) (Sellers and Crompton, 2004; Shi et al., 2012).

In the present study muscle CSAs, ECSAs, and the centroid size of a configuration of landmarks on the skull were used to test the null hypotheses that there are no significant associations between directly measured muscle CSAs, ECSAs, and skull size. If this hypothesis is falsified, ECSA can be considered a reasonable approach for muscle force estimation in humans where actual muscle anatomy cannot be directly observed. If not, this raises methodological issues for functional studies that use masticatory muscle ECSAs.

MATERIALS AND METHODS

This study uses the CT scans of 20 adult individuals, 11 women (aged 29–86 years) and 9 men (aged 38–72 years). The CT data were obtained from the Teaching Hospital of the University of Chile (Hospital Clínico de la Universidad de Chile, Santiago de Chile) under their ethical approval protocol for the use of patient data. The images were taken using a Siemens 64-channel multidetector CT scanner equipped with a STRATON tube (Siemens Somatom Sensation 64, Siemens Healthcare, Erlangen, Germany) during prior medically required investigations, unrelated to this study. The CTs belonged to individuals without skull deformities or orthognatic surgery, and had full or almost-full dentition (i.e. absence of the third molar, occasional 1 to 2 postcanine tooth loss). While MRI is the method of choice for imaging soft tissues, bone is less well represented. Compute tomograms have the advantage of providing good quality representation of both bone and muscle (see van Spronsen et al., 1989; Swash et al., 1995; Mitsiopoulos et al 1998 and ten Dam et al., 2012 for examples). Scans were taken with jaws closed, which is important because this allows landmarking of cranium and mandible in the knowledge that the dentition is always in or very close to occlusion. Clenching, which would impact on muscle cross-sectional area, is unlikely to have occurred during imaging; the imaging protocol dictates that patients are asked to avoid doing this. However, clenching cannot be

ruled out with certainty. Further, the extent of anatomical coverage in the CTs differs among patients, and most of the scans in the sample lack a complete mandible. The primary reconstruction of images for the purpose of selection of suitable scans was performed using Syngo Multimodality Workplace (Siemens Healthcare, Erlangen, Germany). Average voxel size was 0.43 × 0.43 × 1 mm (range 0.39–0.46 × 0.0.39–0.46 × 1 mm). The selected image stacks were then exported as DICOM files for their use in this study.

Three-dimensional skull morphologies were reconstructed from the CT volume stacks using Avizo v. 7.0.1 (Visualization Sciences Group, Burlington). Semiautomated segmentation of CTs based on gray-level thresholds to separate bone from surrounding tissues and air was undertaken. This was then refined where necessary by manual segmentation to ensure complete skeletal anatomical reconstruction of measured regions. Skull surfaces were generated and saved as Wavefront files.

Skull centroid size was computed from 59 facial and neurocranial landmarks placed on the reconstructed 3D surfaces using the EVAN Toolbox v. 1.62 (http://www.evan-society.org/). Due to the lack of a complete mandible in most of the CT images, only the upper half of the ramus was included. The landmarks are shown in Fig. 1 and listed in Table 1. The centroid size of the landmark configuration, was calculated for each individual as the square root of the sum of the squared distances of landmarks from their centroid (Zelditch et al., 2012).

The procedure to estimate the CSA of masticatory muscles from CT scans was based on Weijs and Hillen (1984).

CSA of the Temporalis Muscle

The CSA of the temporalis muscle was estimated by reference to the Frankfurt Plane (FP), which passes through left infraorbitale, and left and right porion. Weijs and Hillen (1984), in a sample of human cranial MRI scans found that the largest temporalis muscle CSAs are found in planes that lie 4 to 16 mm above and parallel to the FP (mean 10 mm). Because skulls vary in size it was decided in this study not to estimate CSA using a sectioning plane at a fixed distance above FP. Instead, the sectioning plane used was standardised to be parallel to the FP and pass through the most medial point of the infratemporal crest. This is identifiable on all specimens and lies well within the region in which Weijs and Hillen (1984) found CSA to vary little (4–16 mm above FP). The CSA was estimated as the average of the muscle cross-sectional area in this sectioning plane and in the two planes (∼1 mm) immediately above it (Fig. 2a,b).

CSA of the Masseter and Medial Pterygoid Muscles

For the masseter and medial pterygoid muscles, the defined sectioning plane was based on the prior work of Weijs and Hillen (1984) who found the largest CSAs of both muscles to lie 25 mm above the mandibular angle. Further, they noted that CSA is largely unchanged in planes ranging between 12 and 30 mm below the zygomatic arch. In the present sample, the mandibular angle could not always be used due to its absence in CT scans. However, the lingula was identifiable in all scans and lies within the range of distances from the zygomatic over which CSA changes little (Weijs and Hillen, 1984). The most posterior point at the base of the lingula was therefore chosen as the reference level for the sectioning plane. Masseter and medial pterygoid CSAs were estimated by averaging CSAs from this sectioning plane and two planes that lie ∼1 mm above and below it (Fig. 2c–e).

For temporalis, masseter, and medial pterygoid, to limit errors associated with the definition of muscle contours, the CSA in each section was measured three times and the values averaged.

The methods used to estimate the CSAs of jaw-elevator muscles from bony proxies are based on O'Connor et al. (2005) and Antón (1999). These estimates are not true cross-sectional areas and as noted earlier, in this paper they are referred to as estimated cross-sectional areas (ECSAs).

Temporalis ECSA corresponds to the area enclosed by the temporal fossa at the zygomatic arch in a plane parallel to the FP. The vertical position of this plane was chosen to be at the level where bony boundaries are most complete to minimise the need for estimation when measuring areas (Fig. 3a,b).

Masseter ECSA is calculated as the product of the width of the muscle and the length of the masseter origin on the zygomatic arch. The width of the muscle was estimated as the medio-lateral distance between the lateral edge of the zygomatic arch projected onto the FP and the projection of the most posterior point at the base of the lingula on the lateral surface of the mandibular ramus (Fig. 3c,d). The length was directly measured on the 3D reconstruction (Fig. 3e).

To control for error, masseter ECSA was calculated three times in each individual and these values were then averaged. The temporalis area was estimated once in each individual because it is traced directly and almost completely along clear bony boundaries. The medial pterygoid muscle was not included in this study because its area of attachment on the mandible was missing in many CT scans.

A preliminary ANOVA showed no significant effect of side (i.e. left/right asymmetry) on the measurements (Table 2). Hence the CSAs and ECSAs corresponding to the right side of the head were used. Skull size is not significantly associated with sex in the sample after Bonferroni correction; therefore sexes were pooled.

As a first step, the square roots of CSAs and ECSAs were calculated. This ensured the dimensions of all variables were the same; mm. These were used in subsequent analyses as were the centroid sizes. The normality of the distributions of (square roots of) muscle CSAs and ECSAs and of centroid sizes was assessed using a Shapiro-Wilks test.

The hypothesis that there is no relationship between muscle CSAs, ECSAs, and skull sizes, was tested through a series of analyses. First, a *t*-test was used to assess the difference between the mean square roots of both CSAs and ECSAs. Second, to assess the significance and degree of association between these measures of area, Pearson's correlation (r) was computed between the CSA and ECSA of each muscle and centroid size to assess potential associations with size. To assess the

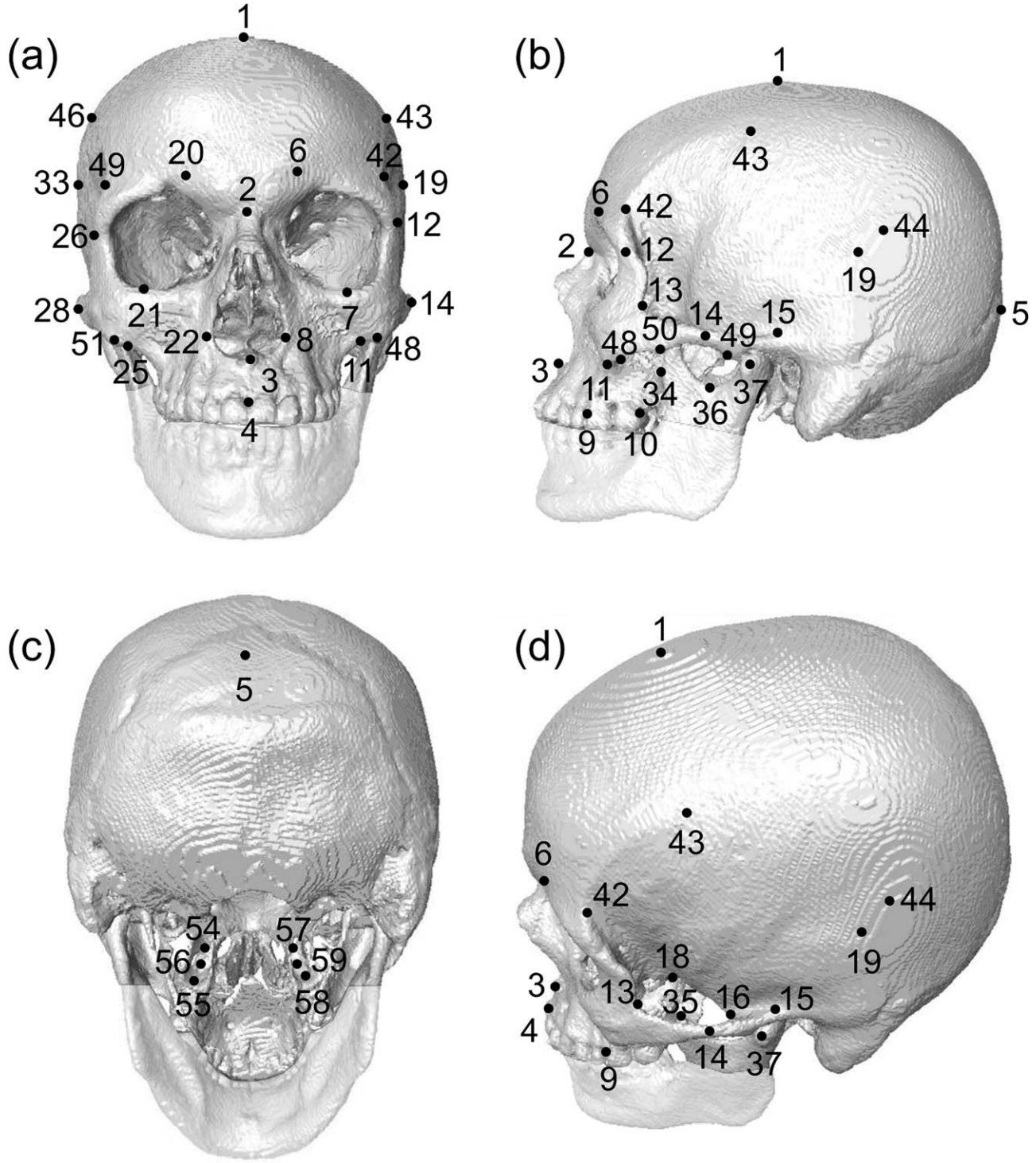

Fig. 1. Reconstructed skull surface and landmarks (described in Table 1). The lower portion of the mandible (in light gray) was absent in most of the sample, and therefore no landmarks were placed on it.

predictability of CSA by ECSA, the regression of CSA on ECSA and the proportion of the total variance of the square root of CSA explained (R^2) by the square root of ECSA and by skull centroid size was separately computed for each muscle.

RESULTS

When CSA versus ECSA for temporalis and masseter are plotted (Fig. 4) the scatters indicate that ECSA does not reliably predict CSA in either muscle. Further, CSA shows a stronger relationship with centroid size than

TABLE 1. Landmarks used to calculate centroid size.

No.	Name	Definition
1	Vertex	Highest point of the cranial vault.
2	Nasion	Intersection between frontonasal and internasal junction.
3	Anterior nasal spine	Tip of the anterior nasal spine.
4	Prosthion	Most buccal and occlusal point of the interalveolar septum between central incisors.
5	Occiput	Most posterior point of the skull.
6&20	Supraorbital torus	Most anterior point of supraorbital ridge.
7&21	Infraorbitale	Most inferior point of the infraorbital ridge.
8&22	Nasal notch	Most lateral part of the nasal aperture.
9&23	First molar	Most buccal and mesial point of the junction of the M1 and the alveolar process. If M1 is absent, the landmark is in the lowest most buccal point of the interalveolar septum between the second premolar and the next molar.
10&24	Last molar	Most buccal and distal point of the junction between the last molar and the alveolar process.
11&25	Zygo-maxillar	Most inferior point of the zygomatico-maxillary junction.
12&26	Fronto-zygomatic	Most lateral point of the fronto-zygomatic junction.
13&27	Fronto-temporal angle	Point at the intersection between frontal and temporal processes of the zygomatic bone.
14&28	Zygomatic arch lateral	Most lateral point of the zygomatic arch.
15&29	Zygomatic root posterior	Most posterior-superior point of the intersection between the zygomatic root and the squama of the temporal bone.
16&30	Zygomatic root anterior	Most anterior point of the intersection between the zygomatic root and the squama of the temporal bone.
17&31	Zygomatic arch medial	Most lateral point on the inner face of the zygomatic arch.
18&32	Infratemporalis crest	Most medial point of the infratemporal crest.
19&33	Eurion	Most lateral point of the cranial vault.
34&38	Coronoid process anterior	Most anterior point of the coronoid process.
35&39	Coronoid process superior	Most superior point of the coronoid process.
36&40	Mandibular notch	Most inferior point of the mandibular notch.
37&41	Condyle	Most lateral point of the condyle.
42&45	Anterior temporal origin	Most anterior point of origin of the temporal muscle in the temporal line.
43&46	Superior temporal origin	Most superior point of origin of the temporal muscle in the temporal line.
44&47	Posterior temporal origin	Most posterior point of origin of the temporal muscle in the temporal line.
48&51	Anterior masseter origin	Most anterior point of origin of the masseter muscle.
49&52	Posterior masseter origin	Most posterior point of origin of the masseter muscle.
50&53	Mid-masseter origin	Midpoint along the area of origin of the masseter muscle.
54&57	Superior pterygoid origin	Most superior point of the origin of the medial pterygoid muscle.
55&58	Inferior pterygoid origin	Most inferior point of origin of the medial pterygoid muscle.
56&59	Mid-pterygoid origin	Midpoint along the area of origin of the medial pterygoid muscle.

does ECSA in the plots of Fig. 5. The descriptive statistics relating to CSAs, ECSAs and skull centroid sizes (CSize) are shown in Table 2. The assessment of accuracy in predicting muscle CSAs from bony proxies showed that the means of CSAs and ECSAs are significantly different in both the temporalis and masseter for both males and females (Table 3). For temporalis, ECSAs are approximately double CSAs. After Bonferroni correction the correlation between temporalis CSAs and ECSAs is significant (Table 3) while that for masseter is not. However, predictability of CSA from ECSA, as assessed by regression, was poor for both muscles.

DISCUSSION

The present study assessed the predictability of masticatory muscle CSAs from bony proxies and skull centroid size in humans. The use of estimates of muscle force based on areas derived from bony proxies is common in mechanical studies of the hominin masticatory system (Demes and Creel, 1988; O'Connor et al., 2005; Wroe et al., 2010). However, previous work in macaques and modern humans has indicated that there are considerable uncertainties in this approach (Antón, 1994, 1999).

Here we provide means and standard deviations of muscle CSAs from a sample of living men and women. The mean CSAs lie within the range of previous published data based on medical images (Weijs and Hillen, 1985b; Hannam and Wood, 1989; van Spronsen et al., 1989). The findings of this study indicate that muscle CSAs and ECSAs differ considerably and the relationship between them is weak and insignificant except for the temporalis muscle. Using MRI instead of CT to measure muscle tissue would not necessarily improve the observed relationship between CSA and ECSA since prior studies have shown comparability of MRI- and CT-based measurements of human masticatory muscle CSAs (van Spronsen et al., 1989) and limb (Mitsiopoulos et al., 1998). Our findings indicate that the use of bony proxies is not a reliable approach to estimating masticatory muscle CSAs in humans. This is in agreement with Antón (1994) who found a low correlation between masseter PCSA and the area estimated from bony proxies in human cadavers. Antón (1994) also found low predictability of temporalis PCSA from the anteroposterior length of the temporal fossa at the zygomatic arch. In

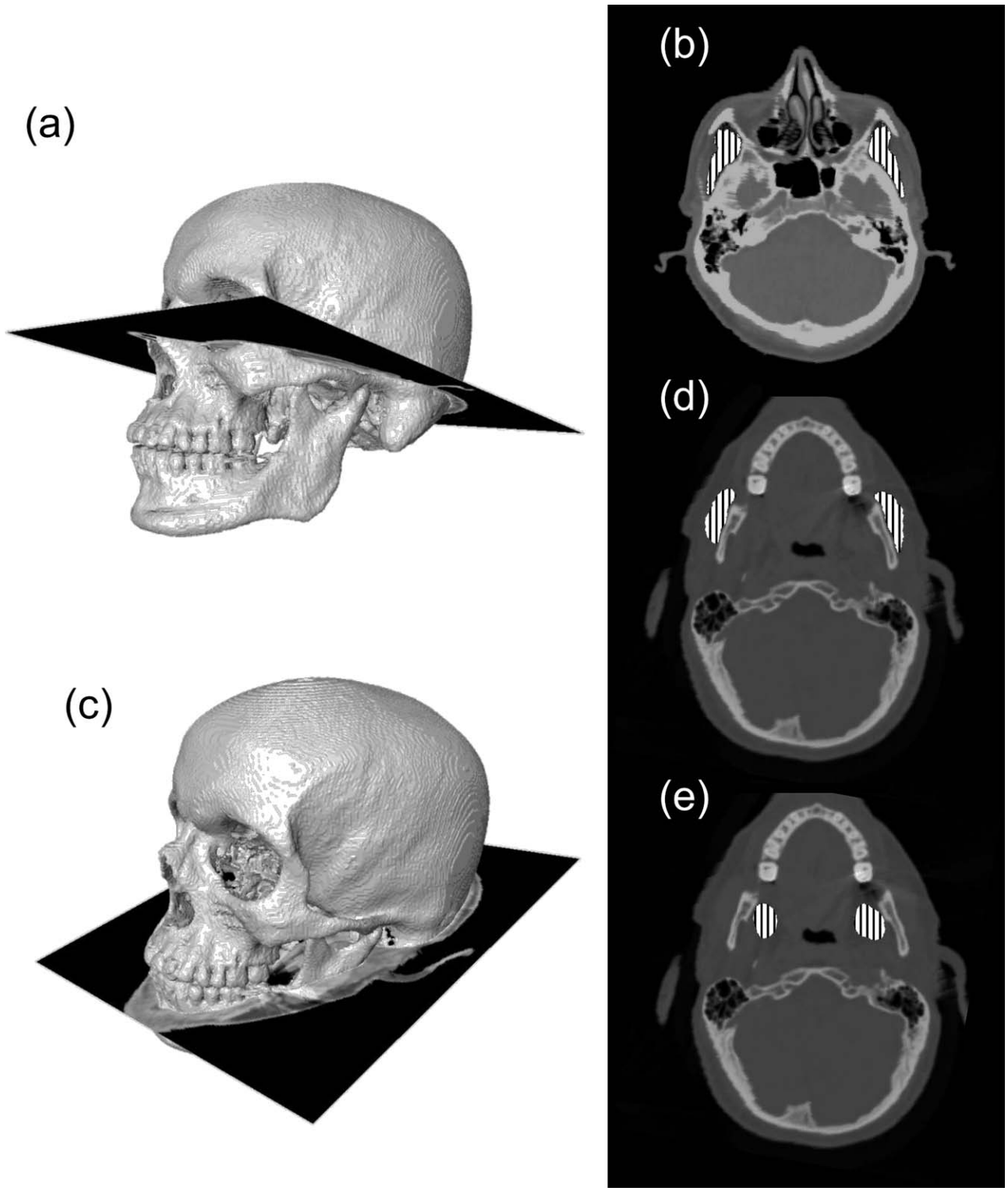

Fig. 2. Selected planes used to measure CSAs of jaw-elevator muscles. (**a**) Plane for (**b**) temporal muscles, (**c**) plane for (**d**) masseter and (**e**) medial pterygoid muscles.

contrast we find that the mean cross-sectional area of temporalis estimated from bony proxies differs from the mean CSA but is significantly correlated with it. Antón (1994) also found a weak relationship in *Macaca* between directly measured PCSA and the estimated areas of temporalis (Antón, 1994) and masseter (Antón, 1999).

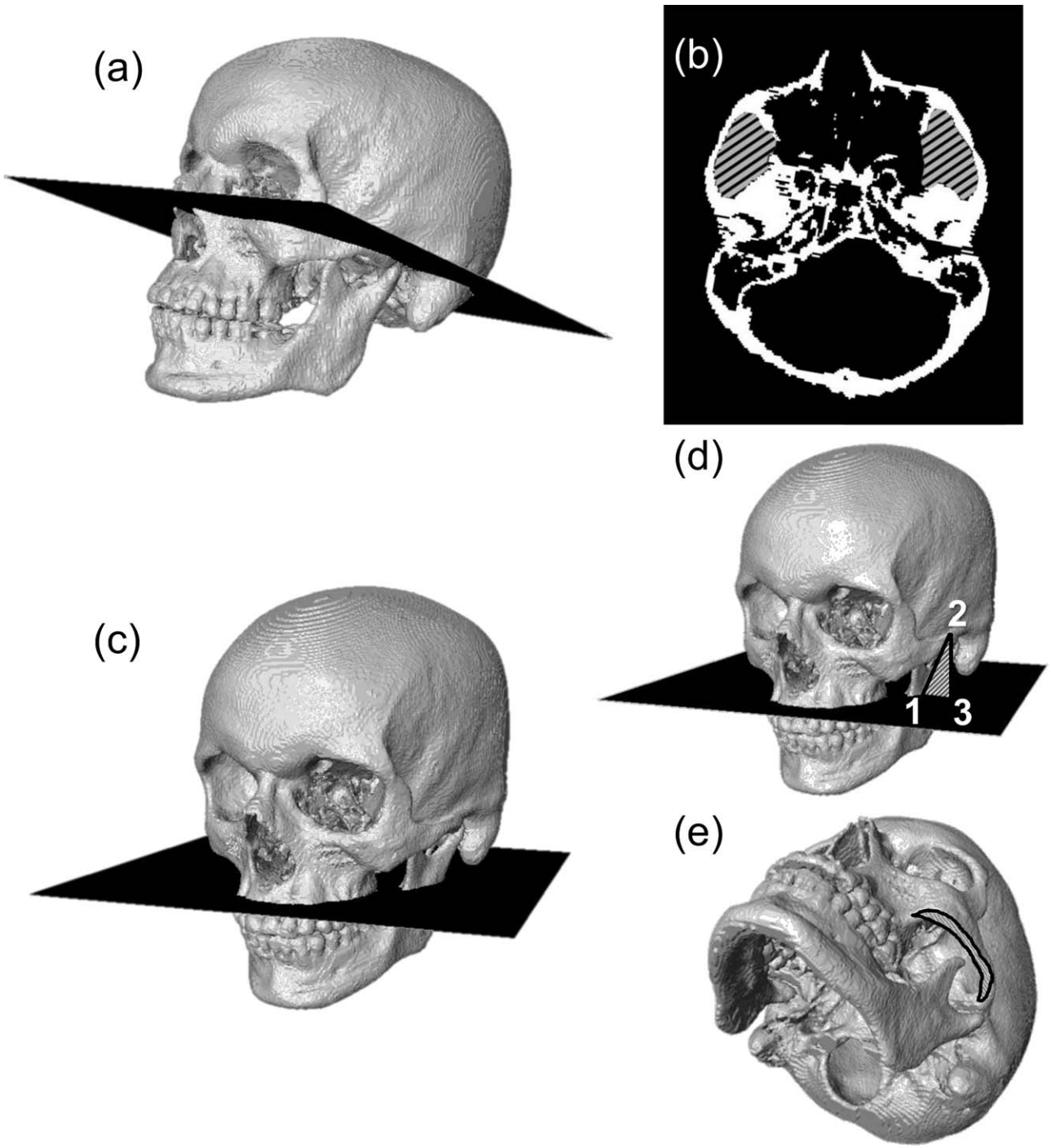

Fig. 3. Planes used for ECSAs. (**a**) Plane for measurement of (**b**) temporalis area, (**c**) reference plane for masseter area, estimated as the product of the width and the length of the masseter origin. (**d**) The "width" of the masseter area was defined as the mediolateral distance from point 1 at the lateral surface of the mandibular ramus to point 3 which is projected vertically from the lateral edge of the zygomatic arch (point 2) onto the plane. (**e**) The "length" of the masseter origin was measured along the muscle scar on the zygomatic arch (highlighted area).

There is also a weak relationship between skull size and both muscle CSA and ECSA. This is in agreement with Weijs and Hillen (1986) who found the highest correlations between CSAs and isolated facial metric traits rather than those related to general size.

To our knowledge, this is the first study to assess the accuracy of human temporalis and masseter CSA estimation from bony proxies in a relatively large sample of living humans. The characteristics of the sample did not allow us to assess the predictability of medial pterygoid

TABLE 2. Descriptive statistics and effect of side and sex on measured CSAs.

			Mean ± SD			Effects of sex and side (*F*-test)			
Variable	Sex	N	Centroid size	Left	Right	Sex	*P*	Side	*P*
Temporalis	F	11	–	475.8 ± 58.6	517 ± 66 511.6 ± 80.6	2.62	0.11	0.05	0.82
CSA (mm^2)	M	9	–	488.5 ± 44.5					
Temporalis	F	11	–	804.2 ± 94.9	798.1 ± 153.7	0.0007	0.98	0.16	0.69
ECSA (mm^2)	M	9	–	815.4 ± 153.8	823.8 ± 148.5				
Masseter	F	11	–	422.8 ± 73.8	432.2 ± 85.3	6.34	0.02	0.09	0.76
CSA (mm^2)	M	9	–	488.6 ± 67.4	494.1 ± 90.4				
Masseter	F	11	–	715.2 ± 80.1	783.3 ± 138.4	6.32	0.02	1.05	0.31
ECSA (mm^2)	M	9	–	729.9 ± 134.1	850.2 ± 113.5				
Medial Pterygoid[a]	F	11	–	302.3 ± 64.7	289.8 ± 63.4	5.68	0.02	0.21	0.65
CSA (mm^2)	M	9	–	344.5 ± 53.6	339 ± 60				
Skull	F	11	491.2 ± 14.2	–	–	4.84	0.04	–	–
CSize (mm)	M	9	504.8 ± 13	–	–				

F = female, M = male, SD = standard deviation.
[a]The CSA values for the medial pterygoid are presented because they may be useful to other workers, but we were unable to estimate areas from bony proxies for comparison because of limited anatomical coverage in the CT scans.

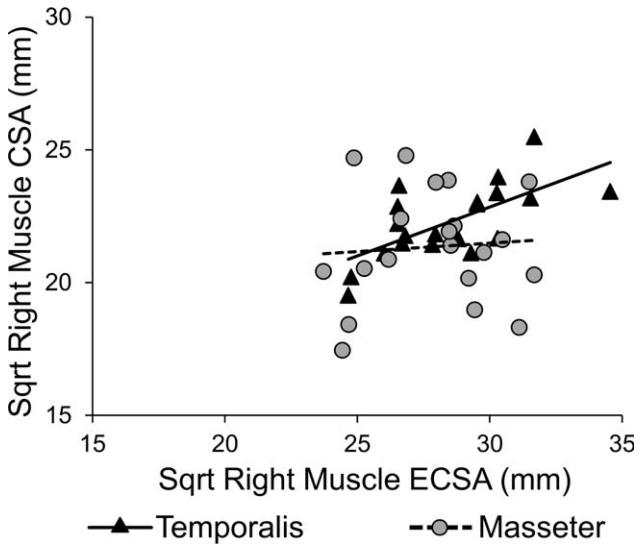

Fig. 4. Relationships between actual muscle CSAs and ECSAs. The least square regression lines of CSA predicted by ECSA are shown for each muscle.

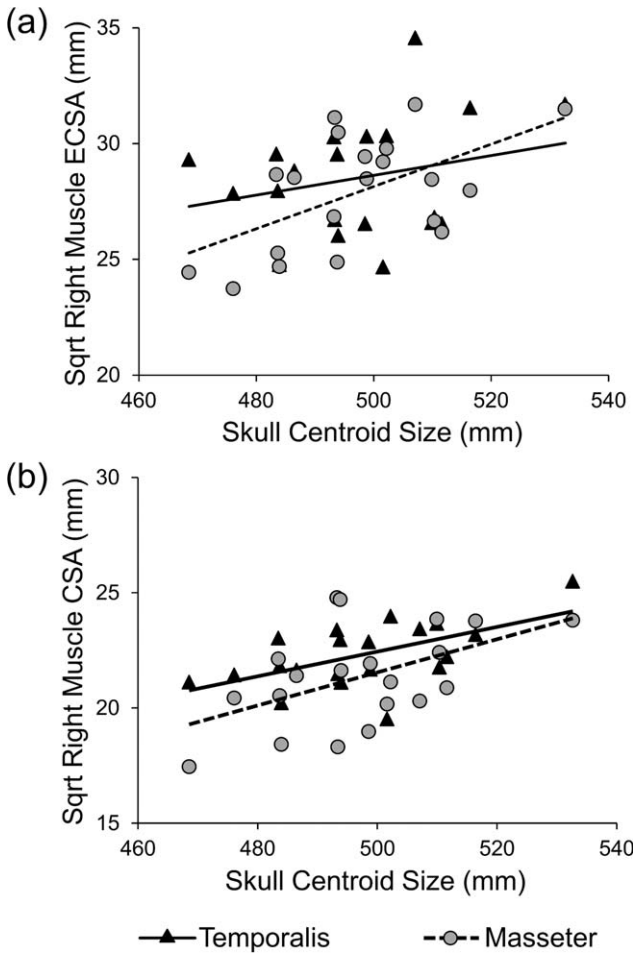

Fig. 5. Relationships between (**a**) ECSAs, (**b**) CSAs and skull centroid size. The regression lines of ECSA or CSA on centroid size are shown for each muscle.

CSA. However, Antón's (1994) study of ten human cadavers found that medial pterygoid PCSA is poorly predicted from bony features, which leads us to expect that this is likely also be the case for CSA. Whether the findings of this study reflect a general pattern in primates, is unknown, although the work of Antón (1994, 1999) suggests that the situation in macaques mirrors what is found in humans. The fact that the degree of jaw-clenching could not be fully controlled in this study may explain the lack of correlation between CSA and ECSA in the masseter (Kiliaridis and Kälebo, 1991). However, clenching would have increased apparent CSA and so reduced the difference between this and ECSA in both masseter and temporalis.

The lack of accuracy in the estimation of masticatory muscle CSAs from bony proxies poses a dilemma for researchers when muscle data are not available, such as in studies of fossils and skeletal material. One solution is to use CSA or PCSA values previously published for the same species (e.g. for humans Reina et al., 2007; Jansen van Rensburg et al., 2012) or related ones (Strait

TABLE 3. Relationship between muscle CSA, ECSA, and skull centroid size.

		Means		Correlation		Regression	
Muscle	Variables *Y* vs. *X*	*t*	*P*	r	*P*	*F*(*x*)	R^2
Temporalis	CSA vs. ECSA	9.63	**<0.001**	0.66	**0.001**	$y = 0.37x + 11.81$	0.45
	CSA vs. CSize	–	–	0.58	0.008	$y = 0.05x - 4.31$	0.33
	ECSA vs. CSize	–	–	0.25	0.28	$y = 0.04x + 7.32$	0.06
Masseter	CSA vs. ECSA	9	**<0.001**	0.073	0.76	$y = 0.06x + 19.58$	0.01
	CSA vs. CSize	–	–	0.51	0.02	$y = 0.07x - 14.37$	0.26
	ECSA vs. CSize	–	–	0.56	0.01	$y = 0.09x - 17.51$	0.31

Data correspond to the right side of the head. Significant *P* values after Bonferroni correction (significant *P* value 0.05/6 = 0.0083), are shown in bold.

et al., 2009; Smith et al., 2015). Nevertheless, attention must be paid to possible differences in muscle architecture between related primate taxa due to functional differences, for example, in feeding behavior (Anapol et al., 2008; Taylor et al., 2009) which could lead to errors in PCSA and hence, force magnitude estimation. How errors impact on resulting strain magnitudes (degree of deformation) and distributions (mode of deformation) has recently been explored in a macaque model by Fitton et al. (2012). They found that with quite large variations in muscle forces, that left the bite force unchanged, the magnitude and mode of deformation of the facial skeleton distant from the zygomatic arch was little affected. The magnitude of deformation of the zygomatic arch is, however, very dependent on masseter force. Ross et al. (2005) in a sensitivity analysis against *in vivo* data from macaques found that the total applied muscle force has a larger effect on FEA results, in terms of overall strain magnitudes, than varying the relative magnitudes of force among muscles. Thus, where muscle data can only be obtained by estimation from bony proxies it is necessary to carry out sensitivity analyses, varying force magnitudes and relative forces among muscles, to assess the likely impact of errors in model strain magnitudes and distribution.

In conclusion, the results of this study suggest that, although the temporalis CSA correlates significantly with ECSA from bony proxies, jaw-elevator muscle CSAs cannot be reliably estimated from bony proxies in humans. Sampling of a wider range of species and the inclusion of medial pterygoid muscles is called for to better understand how generalizable these findings are. The finding of low predictability of CSA and so muscle force from bony proxies also calls for further studies such as those of Ross et al. (2005) and Fitton et al. (2012) in macaques to assess the impact of variations in masticatory muscle force on mechanical analyses of human fossils and archaeological material.

ACKNOWLEDGEMENTS

The authors thank Williams Astudillo (Hospital Clínico Universidad de Chile) for his help during CT data collection.

LITERATURE CITED

Anapol F, Shahnoor N, Ross C. 2008. Scaling of reduced physiologic cross-sectional area in primate muscles of mastication. In: Vinyard C, Ravosa M, Wall C, editors. Primate craniofacial function and biology. New York: Springer. p 201–216.

Antón SC. 1990. Neandertals and the anterior dental loading hypothesis: a biomechanical evaluation of bite force production. Kroeber Anthropol Soc Pap 71-72:67–76.

Antón SC. 1994. Masticatory muscle architecture and bone morphology in primates. Berkeley, CA: University of California.

Antón SC. 1999. Macaque masseter muscle: internal architecture, fiber length and cross-sectional area. Int J Primatol 20:441–462.

Cox PG, Jeffery N. 2011. Reviewing the morphology of the jaw-closing musculature in squirrels, rats, and guinea pigs with contrast-enhanced micro-CT. Anat Rec 294:915–928.

Demes B, Creel N. 1988. Bite force, diet, and cranial morphology of fossil hominids. J Hum Evol 17:657–670.

DiGirolamo DJ, Kiel DP, Esser KA. 2013. Bone and skeletal muscle: neighbors with close ties. J Bone Miner Res 28:1509–1518.

Fitton L, Shi J, Fagan M, O'Higgins P. 2012. Masticatory loadings and cranial deformation in *Macaca fascicularis*: a finite element analysis sensitivity study. J Anat 221:55–68.

Gröning F, Fagan MJ, O'Higgins P. 2012. Modeling the human mandible under masticatory loads: which input variables are important? Anat Rec 295:853–863.

Hannam A, Wood W. 1989. Relationships between the size and spatial morphology of human masseter and medial pterygoid muscles, the craniofacial skeleton, and jaw biomechanics. Am J Phys Anthropol 80:429–445.

Jansenvan Rensburg GJ, Wilke DN, Kok S. 2012. Human skull shape and masticatory induced stress: objective comparison through the use of non-rigid registration. Int J Numer Method Biomed Eng 28:170–185.

Kiliaridis S, Kälebo P. 1991. Masseter muscle thickness measured by ultrasonography and its relation to facial morphology. J Dent Res 70:1262–1265.

Koolstra J, van Eijden T, Weijs W, Naeije M. 1988. A three-dimensional mathematical model of the human masticatory system predicting maximum possible bite forces. J Biomech 21:563–576.

Kupczik K, Dobson CA, Crompton RH, Phillips R, Oxnard CE, Fagan MJ, O'Higgins P. 2009. Masticatory loading and bone adaptation in the supraorbital torus of developing macaques. Am J Phys Anthropol 139:193–203.

Martin DC, Medri MK, Chow RS, Oxorn V, Leekam RN, Agur AM, McKee NH. 2001. Comparing human skeletal muscle architectural parameters of cadavers with in vivo ultrasonographic measurements. J Anat 199:429–434. [PMC][11693303]

Mioche L, Bourdiol P, Monier S, Martin J-F, Cormier D. 2004. Changes in jaw muscles activity with age: effects on food bolus properties. Physiol Behav 82:621–627.

Mitsiopoulos N, Baumgartner RN, Heymsfield SB, Lyons W, Gallagher D, Ross R. 1998. Cadaver validation of skeletal muscle measurement by magnetic resonance imaging and computerized tomography. J Appl Physiol 85:115–122.

Moss ML. 1962. The functional matrix. In: Vistas in orthodontics. Philadelphia: Lea & Febiger. p 85–98.

Newton J, Yemm R, Abel R, Menhinick S. 1993. Changes in human jaw muscles with age and dental state. Gerodontology 10:16–22.

O'Connor CF, Franciscus RG, Holton NE. 2005. Bite force production capability and efficiency in neandertals and modern humans. Am J Phys Anthropol 127:129–151.

Rayfield EJ. 2007. Finite element analysis and understanding the biomechanics and evolution of living and fossil organisms. Annu Rev Earth Planet Sci 35:541–576.

Reina JM, García-Aznar JM, Domínguez J, Doblaré M. 2007. Numerical estimation of bone density and elastic constants distribution in a human mandible. J Biomech 40:828–836.

Ross CF, Patel BA, Slice DE, Strait DS, Dechow PC, Richmond BG, Spencer MA. 2005. Modeling masticatory muscle force in finite element analysis: sensitivity analysis using principal coordinates analysis. Anat Rec a Discov Mol Cell Evol Biol 283:288–299.

Scott JH. 1957. Muscle growth and function in relation to skeletal morphology. Am J Phys Anthropol 15:197–234.

Seeman E. 2001. Sexual dimorphism in skeletal size, density, and strength. J Clin Endocrinol Metab 86:4576–4584.

Sellers WI, Crompton RH. 2004. Using sensitivity analysis to validate the predictions of a biomechanical model of bite forces. Ann Anat 186:89–95.

Shi J, Curtis N, Fitton LC, O'Higgins P, Fagan MJ. 2012. Developing a musculoskeletal model of the primate skull: predicting muscle activations, bite force, and joint reaction forces using multibody dynamics analysis and advanced optimisation methods. J Theor Biol 310:21–30.

Smith AL, Benazzi S, Ledogar JA, Tamvada K, Pryor Smith LC, Weber GW, Spencer MA, Lucas PW, Michael S, Shekeban A, Al-Fadhalah K, Almusallam AS, Dechow PC, Grosse IR, Ross CF, Madden RH, Richmond BG, Wright BW, Wang Q, Byron C, Slice DE, Wood S, Dzialo C, Berthaume MA, van Casteren A, Strait DS. 2015. The feeding biomechanics and dietary ecology of *Paranthropus boisei*. Anat Rec 298:145–167.

Strait DS, Weber GW, Neubauer S, Chalk J, Richmond BG, Lucas PW, Spencer MA, Schrein C, Dechow PC, Ross CF. 2009. The feeding biomechanics and dietary ecology of *Australopithecus africanus*. 106:2124–2129. PNAS

Swash M, Brown MM, Thakkar C. 1995. CT muscle imaging and the clinical assessment of neuromuscular disease. Muscle Nerve 18:708–714.

Taylor AB, Eng CM, Anapol FC, Vinyard CJ. 2009. The functional correlates of jaw-muscle fiber architecture in tree-gouging and nongouging callitrichid monkeys. Am J Phys Anthropol 139:353–367.

tenDam L, van der Kooi AJ, van Wattingen M, de Haan RJ, de Visser M. 2012. Reliability and accuracy of skeletal muscle imaging in limb-girdle muscular dystrophies. Neurology 79:1716–1723.

vanEijden T, Korfage J, Brugman P. 1997. Architecture of the human jaw-closing and jaw-opening muscles. Anat Rec 248:464–474.

vanSpronsen P, Weijs W, Valk J, Prahl-Andersen B, Van Ginkel F. 1989. Comparison of jaw-muscle bite-force cross-sections obtained by means of magnetic resonance imaging and high-resolution CT scanning. J Dent Res 68:1765–1770.

vanSpronsen P, Weijs W, Valk J, Prahl-Andersen B, van Ginkel F. 1992. A comparison of jaw muscle cross-sections of long-face and normal adults. J Dent Res 71:1279.

Weijs W, Hillen B. 1984. Relationship between the physiological cross-section of the human jaw muscles and their cross-sectional area in computer tomograms. Acta Anat 118:129–138.

Weijs W, Hillen B. 1985a. Cross-sectional areas and estimated intrinsic strength of the human jaw muscles. Acta Morphol Neer Sc 23:267–274.

Weijs W, Hillen B. 1986. Correlations between the cross-sectional area of the jaw muscles and craniofacial size and shape. Am J Phys Anthropol 70:423–431.

Weijs WA, Hillen B. 1985b. Physiological cross-section of the human jaw muscles. Cells Tissues Organs 121:31–35.

Wroe S, Ferrara TL, McHenry CR, Curnoe D, Chamoli U. 2010. The craniomandibular mechanics of being human. Proc R Soc B 277: 3579–3586.

Yoshikawa T, Mori S, Santiesteban A, Sun T, Hafstad E, Chen J, Burr DB. 1994. The effects of muscle fatigue on bone strain. J Exp Biol 188:217–233.

Zelditch ML, Swiderski DL, Sheets HD. 2012. Geometric morphometrics for biologists: a primer. San Diego: Elsevier Academic Press.